Theoretical basis of parametric-resonance-based atomic force microscopy

G. Prakash
The Birck Nanotechnology Center, and Department of Physics, Purdue University, West Lafayette, Indiana 47907, USA

S. Hu
Veeco Metrology, Inc., Santa Barbara, California 93117, USA

A. Raman
The Birck Nanotechnology Center and School of Mechanical Engineering, Purdue University, West Lafayette, Indiana 47907, USA

R. Reifenberger
The Birck Nanotechnology Center, and Department of Physics, Purdue University, West Lafayette, Indiana 47907, USA

(Received 18 July 2008; revised manuscript received 29 January 2009; published 19 March 2009)

Parametric resonance underpins the physics of swings, resonant surface waves, and particle traps. There is increasing interest in its potential applications in atomic force microscopy (AFM). In this paper, the dynamics of parametrically resonant microcantilevers for high sensitivity imaging and force spectroscopy applications is investigated theoretically. Detailed numerical parametric-resonance simulations are performed to understand how the microcantilever amplitude varies with tip-sample separation, the tip-sample interaction, and the scanning dynamics of a microcantilever probe. We find three key advantages of a parametrically resonant microcantilever for AFM applications: (a) the reduction in ringing effects near feature edges that occur for high-Q microcantilevers; (b) an increase in the scanning speed while maintaining a low tip-sample interaction force while imaging; and (c) an enhanced sensitivity to long-range magnetic and electrostatic force gradients acting between the tip and the sample. Experimental results are presented with an aim to clearly identify the advantages and disadvantages that parametric resonance offers for scanning probe applications.

DOI: 10.1103/PhysRevB.79.094304 PACS number(s): 68.37.Ps, 68.37.Rt, 05.45.−a

I. INTRODUCTION

A common problem encountered in the use of dynamic atomic force microscopy (dAFM) is the broad resonance that is characteristic of the microcantilever oscillation. Typically, resonance Q factors of $\sim 100-500$ are achieved under ambient conditions. This limits the force sensitivity in dAFM defined as the peak tip-sample interaction force (the imaging force) applied by the oscillating tip on the sample. To improve sensitivity and reduce the imaging force, Q control[1–5] has been introduced in dAFM wherein electronic feedback circuits reduce the effective damping coefficient of the microcantilever system, increasing the force sensitivity and decreasing the imaging force.[4,5] However Q control also reduces the system bandwidth, resulting in a long transient response, slow scanning speeds, and unwanted "ringing" effects.[1,6] Consequently there is a need for nonconventional means to excite and resonate dAFM microcantilevers to reduce the imaging force and to improve force sensitivity without sacrificing scan speed.

One recent development in the area of nonconventional cantilever excitation has been the use of parametric excitation and parametric resonance in dAFM.[7–10] Parametric excitation and resonance underpin many physical phenomena including the motion of surface waves, particle traps,[11,12] and children's swings.[13] More recently, applications of parametric resonance to microelectromechanical and nanoelectromechanical systems have been reported.[14,15]

Before proceeding, it is helpful to distinguish between *parametric excitation* and *parametric resonance*. Parametric *excitation* is a nonconventional excitation that is achieved by varying periodically a system parameter such as the stiffness or mass of an oscillator as opposed to applying a periodic external force to it. Under certain conditions, parametric excitation can lead to parametric *resonance* where the oscillator begins to vibrate with significant amplitude. For instance, when the frequency of parametric excitation is near twice the natural frequency of an oscillator, and if the strength or gain of the parametric excitation is above a threshold value, then *principal parametric resonance* is said to occur in that oscillator. Other secondary parametric resonances are also possible depending on the frequency ratio between the parametric excitation and the natural frequency of the oscillator and the parametric gain.[16]

Several methods have been proposed to introduce parametric excitation and resonance in microcantilevers. Moreno-Moreno *et al.*[7] implemented parametric excitation and resonance in microcantilevers by means of electronic feedback to the base of the microcantilever. Requa and Turner[9] implemented parametric excitation and resonance utilizing the Lorentz force by passing an alternating current through a microcantilever placed in a uniform magnetic field. Patil and Dharmadhikari[10] investigated parametric excitation and resonance by periodically moving the substrate instead of the microcantilever to produce a periodic modulation of van der Waals force. Ouisse *et al.*[8] theoretically investigated parametric excitation and resonance using the electrostatic force gradient near a biased microcantilever.

Parametric excitation has been previously proposed in sensors and scanning probe microscopy (SPM) applications as a mechanical preamplifier. Rugar and Grutter[17] achieved parametric excitation by generating an electrostatic force

gradient near a microcantilever to demonstrate thermomechanical noise squeezing. Dougherty *et al.*[18] used a time varying magnetic moment to parametrically excite a microcantilever fitted with a magnetic particle at the free end. Dâna *et al.*[19] achieved parametric excitation by mechanically modifying the second-order nonlinear stiffness of a microcantilever. However, the gain in these cases was below the threshold value and consequently, parametric resonance was not attained; instead parametric amplification was demonstrated.

In this paper, we analyze the different methods of parametric excitation to achieve parametric resonance in microcantilevers and use mathematical models to better understand the advantages that parametrically resonant dAFM probes might offer for advanced SPM applications. We compare our simulation results for parametrically excited microcantilevers to (a) the simulation results of a conventionally excited microcantilever, (b) the simulation results of a Q-controlled microcantilever, and (c) with other experimental results, with an aim to clearly identify the advantages and disadvantages that each technique offers for SPM.

II. THEORY

Consider a sharp probe tip ("tip" hereafter) attached at the free end of a microcantilever. The equation of motion for the free end of the microcantilever, oscillating in its first eigenmode about its equilibrium position, at a distance Z_0 from the sample is given by[20]

$$\ddot{q} + \frac{\omega_0}{Q}\dot{q} + \omega_0^2 q = \frac{1}{m}f(t) + \frac{1}{m}F_{\mathrm{ts}}(z), \tag{1}$$

where q represents the instantaneous tip displacement from its equilibrium position, $\dot{q}$ and $\ddot{q}$ represent the tip velocity and acceleration, respectively, Q is the quality factor of the fundamental eigenmode of the microcantilever, ω_0 is the natural frequency of the first eigenmode, $f(t)$ is the mode dependent (modal) driving force, m is the effective modal mass, $F_{\mathrm{ts}}(z)$ is the interaction force between the tip and sample, and $z(t)=Z_0+q(t)$ is the instantaneous tip-sample separation.

Parametric excitation of the microcantilever is achieved by adjusting the modal driving force $f(t)$ so as to modulate the stiffness of the microcantilever. For instance, Ouisse *et al.*[8] reported the parametric excitation of the microcantilever by using electrostatic interactions. An alternating voltage $V(t)=V_0\cos(\omega_0 t)$, where V_0, the amplitude of an alternating voltage applied to the substrate, excites a biased metallic microcantilever positioned nearby so that the driving force is given by $f(t)=\frac{1}{2}\frac{\partial C}{\partial z}V^2$, where C is the capacitance between tip and sample. After expanding $f(t)$ in Taylor's series about $z=Z_0$, Eq. (1), after rearranging terms, becomes

$$\ddot{q} + \frac{\omega_0}{Q}\dot{q} + \omega_0^2\left(1 - \frac{1}{2m\omega_0^2}\frac{\partial^2 C}{\partial z^2}\bigg|_{z=Z_0} V(t)^2\right)q = \frac{1}{2m}\frac{\partial C}{\partial z}\bigg|_{z=Z_0} V(t)^2 + \frac{F_{\mathrm{ts}}(z)}{m}. \tag{2}$$

The left-hand side of Eq. (2) shows that the applied alternating voltage $V(t)$ can be used to modulate periodically the equivalent stiffness of the oscillator [all the terms multiplying q on the left-hand side of Eq. (2)]. If the right-hand side of Eq. (2) is neglected we recover the linearized damped Mathieu's equation,[21]

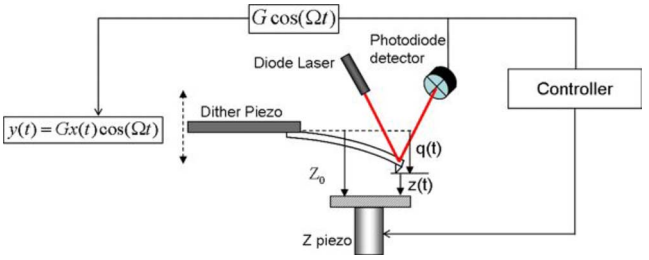

FIG. 1. (Color online) A diagram of the feedback scheme required to implement a parametric AFM. Parametric resonance is achieved when the excitation frequency applied to the dither piezo is twice the natural frequency ($\Omega \sim 2\omega_0$) and the gain G is greater than the threshold value ($G > G_{\mathrm{th}}$).

$$\ddot{q} + \frac{\omega_0}{Q}\dot{q} + \omega_0^2[1 - g(t)]q = 0, \tag{3}$$

where $g(t)=\frac{V_0^2}{4m\omega_0^2}\frac{\partial^2 C}{\partial z^2}\big|_{z=Z_0}(1+\cos 2\omega_0 t)$ is a harmonic function of time. Thus electrostatic forcing can be conveniently used to create parametric excitation especially if the microcantilever is relatively close to the surface.

Requa and Turner[9] reported on parametric excitation using the electromagnetic Lorentz force. A U-shaped conducting microcantilever is placed in a uniform magnetic field and an alternating current is passed through the microcantilever. The lever experiences a periodic Lorentz force $p(t)$ along its longitudinal axis, thus alternating the compressive axial stress in the microcantilever. The periodic compressive axial stress in turn periodically modulates the effective out-of-plane bending stiffness of the microcantilever thus parametrically exciting the structure. It has been shown that the underlying linearized equation of motion that governs the Lorentz force excited microcantilever is precisely the linear damped Mathieu's equation[9] [Eq. (3)].

Finally Moreno-Moreno *et al.*[7] reported the parametric excitation using an electronic feedback mechanism as shown in Fig. 1. In this case the microcantilever deflection is fed back electronically to the microcantilever dither piezo after multiplying by $\cos(\Omega t)$ and a gain factor (G). Here, Ω is the excitation frequency which is close to $2\omega_0$. It has been shown[7] that in this case, the underlying equation of motion is Mathieu's equation [Eq. (3)]. Thus the linearized Mathieu equation commonly describes the linear physics of parametrically excited microcantilevers regardless of the specific method of excitation.

It is well known that the nontrivial solutions of the damped linearized Mathieu equation [Eq. (3)] can grow in amplitude and become unbounded when $g(t)$ varies with a frequency close to double that of the natural frequency ω_0 (principal parametric resonance) and the magnitude of parametric excitation is larger than a threshold value.[22] In reality many attendant nonlinearities in the system conspire to satu-

rate the amplitude to a steady-state value under conditions of principal parametric resonance. The nature of the nonlinearities is diverse; for instance, Requa and Turner[9] considered elastic nonlinearities due to large deformations of the microcantilever (both curvature and inertial). Moreno-Moreno *et al.*[7] considered nonlinear hydrodynamic damping. In the case of electrostatically induced parametric resonance, the nonlinear electrostatic forces could also affect the steady-state amplitude. As important as these nonlinearities are for determining the microcantilever oscillation amplitude far from the sample, in AFM applications when the tip comes close to the sample, the nonlinearities with the largest force gradient are due to tip-sample interaction forces. Thus when the tip begins to interact with the sample the other nonlinearities are negligible. It follows that when the microcantilever is far from the sample, its "free" vibration amplitude (A_0) must be determined by the other nonlinearities in the system. The free vibration amplitude in AFM is usually small ($\sim$100 nm or lower) to minimize the tip forces exerted on the sample. This desire for small forces is yet another reason why structural nonlinearities are usually small when compared to the tip-sample interaction nonlinearities.

In what follows we specifically choose to consider a nonlinear hydrodynamic damping model so as to achieve finite steady-state amplitude before the microcantilever begins to interact with the sample. As we will show, this nonlinear model captures very well the experimental data of recent work on parametrically excited microcantilevers in dAFM.[7] In principle, other nonlinearities can be included, but as we will see the fundamental physics of the problem is determined by the tip-sample interaction forces.

Accordingly a modified version of Eq. (1) will serve as the nominal model for the dynamics of parametrically resonant AFM probes interacting with the sample, regardless of the mechanism used for inciting the parametric resonance,

$$\ddot{q} + \omega_0^2(1 - G\cos\Omega t)q + \frac{\omega_0}{Q}\dot{q} + \frac{\alpha}{m}|\dot{q}|\dot{q} = \frac{1}{m}F_{\mathrm{ts}}(z), \quad (4)$$

where α is the coefficient of nonlinear hydrodynamic damping that is determined by comparing the experimental free vibration amplitude to the predicted one, G represents gain, and Ω represents the excitation frequency. For a parametrically resonating microcantilever implemented using electronic feedback,[7] the gain (G) is the amplitude of the harmonic signal multiplied by the microcantilever oscillation signal (q) before feeding it back to the base of the microcantilever.

For a parametrically resonating microcantilever using the electrostatic force,[8] G is defined as $\frac{V_0^2}{4m\omega_0^2}\frac{\partial^2 C}{\partial z^2}\big|_{z=Z_0}$. The amplitude of the harmonic signal, obtained from Taylor's expansion, can be controlled by changing V_0 and Z_0. For a parametrically resonating microcantilever using the Lorentz force,[9] the gain is defined as the amplitude of the periodically modifying axial compressive force $p(t)$, which is controlled by changing the alternating current. Ω is the excitation frequency, which is the frequency of the harmonic signal multiplied with the oscillation signal of the microcantilever before feeding it back to the dither piezo (as in Ref. 7), twice the frequency of the alternating bias voltage (as in Ref. 8), and the frequency of alternating current (as in Ref. 9). The threshold gain, $G_{\mathrm{th}}=2/Q$, is the minimum gain of excitation signal required to overcome the damping in the system and to achieve self-sustained oscillation. When Ω is close to $2\omega_0$ and G is more than G_{th}, the microcantilever resonates parametrically (primary parametric resonance).

The short-range tip-sample interaction force (F_{ts}) is assumed to include the van der Waals force and the Derjaguin-Muller-Toporove (DMT) contact force.[23] This serves as a nominal tip-sample interaction model appropriate for hard contacts with low tip-sample adhesion. F_{ts} depends on the instantaneous tip-sample gap, $z(t)$, and is given by

$$F_{\mathrm{ts}}(z) = \begin{cases} -\dfrac{AR}{6z^2} & \text{for } z > a_0 \\ -\dfrac{AR}{6a_0^2} + \dfrac{4}{3}E^*\sqrt{R}(a_0 - z)^{3/2} & \text{for } z \le a_0, \end{cases} \quad (5)$$

where A is the Hamaker constant between the tip and the sample, R is the effective tip radius, E^* is the effective elastic modulus of tip-sample combination, and a_0 is intermolecular distance at which contact is initiated.

In order to compare the potential benefits of the parametrically resonant microcantilever in AFM (parametric AFM) over existing methods, the tip dynamics of parametrically resonant microcantilevers are compared with conventionally excited and Q-controlled microcantilevers at resonance. For instance, the equation of motion of a conventional acoustically excited microcantilever is given as[20]

$$\ddot{q} + \frac{\omega_0}{Q}\dot{q} + \omega_0^2 q = \frac{1}{m}F_{\mathrm{ts}}(z) + \omega^2 YB\cos(\omega t), \quad (6)$$

where Y is the amplitude of the base motion, $B=1.566$ is the modal parameter for the first eigenmode, and ω is the excitation frequency. Q-controlled AFM is modeled simply as a tunable quality factor Q_{eff} which can be different from the "natural" Q factor,[4,5]

$$\ddot{q} + \frac{\omega_0}{Q_{\mathrm{eff}}}\dot{q} + \omega_0^2 q = \frac{1}{m}F_{\mathrm{ts}}(z) + \omega^2 YB\cos(\omega t). \quad (7)$$

In order to achieve resonance in the conventional [Eq. (6)] and Q-controlled [Eq. (7)] models, ω is set to be equal to ω_0.

Parametric excitation is possible using both acoustic[7] and nonacoustic[8,9] excitations. Equation (4) is the theoretical model for parametric excitation irrespective of the method (acoustic or nonacoustic) chosen to do so. In this paper we compare the parametric excitation of a microcantilever (acoustic or nonacoustic) with an acoustically excited conventional and a Q-controlled microcantilever. For a moderate to high Q factor, the frequency response of microcantilevers using acoustic or nonacoustic excitation is not very different near resonance. Hence it is valid to compare the parametric excitation model developed in Eq. (4) with the acoustically excited conventional [Eq. (6)] and Q-controlled [Eq. (7)] models having the same free vibration amplitude as for the parametric case at resonance.

TABLE I. Parameters and properties of Si microcantilever and HOPG sample used in numerical simulation.

Description	Value
Tip radius	$R=10$ nm
Microcantilever length	$L=125$ μm
Microcantilever width	$b=30$ μm
Microcantilever thickness	$h=4$ μm
Microcantilever material density	$\rho_c=2300$ kg/m^3
Microcantilever Young's modulus	$E_c=130$ GPa
Effective elastic modulus (sample)	$E^*=10.2$ GPa
Natural frequency	$f_0=310.9$ kHz
Quality factor (natural)	$Q=520$
Quality factor (Q controlled)	$Q_{\text{eff}}=6000$
Hamaker constant (Si-HOPG)	$A=2.96\times10^{-19}$ J
Intermolecular distance	$a_0=0.3813$ nm
Feedback gain (parametric excitation)	$G=1.0139G_{\text{th}}$

III. NUMERICAL SIMULATIONS

The theoretical models for the microcantilever interacting with a sample in parametrically resonant, Q-controlled, and conventional AFMs are given by Eqs. (4), (6), and (7), respectively. These equations are numerically integrated using the FORTRAN based DDASKR routine with root finding algorithm implemented to accurately integrate the nonsmooth tip-sample interaction forces. The DDASKR routine is based on DASPK, a differential algebraic equations software package.[24–26]

The numerical integrations are simulated for a highly oriented pyrolytic graphite (HOPG) sample and a silicon microcantilever having a resonance frequency of 286.6 kHz. The microcantilever stiffness and natural Q factor of 520 are chosen to replicate the experimental results of prior work.[7] Table I lists the specific tip-sample and microcantilever properties chosen for the simulations. A very small numerical tolerance (10^{-12}) and a very small time step (1000 points per cycle) are chosen to ensure accurate integration results. The steady-state solutions are obtained after discarding the initial transient cycles (5000 cycles for conventional and 10 000 and 100 000 for Q-controlled and for parametrically excited microcantilevers, respectively). Amplitude and phase of the microcantilever oscillation are calculated with respect to the harmonic signal at half of the excitation frequency using a Fourier transform over ten oscillation cycles, corresponding to a lock-in time constant of 32 μs.

For parametrically resonant microcantilevers, three kinds of simulations are performed, namely, (a) *frequency response* (*tuning curves*) far from the sample, where the amplitude response is computed when the excitation frequency ($\Omega \sim 2\omega_0$) is swept across twice the resonance frequency of the microcantilever, (b) *approach curves* are simulated, where the amplitude response is computed by continuously changing Z_0 with the parametric excitation frequency fixed at $\Omega = 2\omega_0$, and (c) *surface scans* are simulated where the amplitude of an oscillating microcantilever is computed as the tip encounters surface features at a fixed parametric excitation frequency $\Omega=2\omega_0$ while maintaining a fixed equilibrium tip-sample separation Z_0. *Open loop scans* (no feedback) are performed to study the transient behavior of a resonating microcantilever under parametric excitation. In an open-loop scan no correction is made to the piezoheight when the microcantilever undergoes transient oscillations after encountering a surface feature. The study of such transient behavior is essential to design a scanning controller; the fewer the transients in an open-loop scan, the easier it is to scan faster.

Such simulations for the parametrically resonant microcantilever are systematically compared with similar simulations performed for conventional and Q-controlled excitations. However in comparing the parametrically resonant and Q-controlled simulations, it is essential to choose an effective Q factor (Q_{eff}) for the Q-controlled case that makes a fair comparison possible. This issue is discussed in Sec. IV.

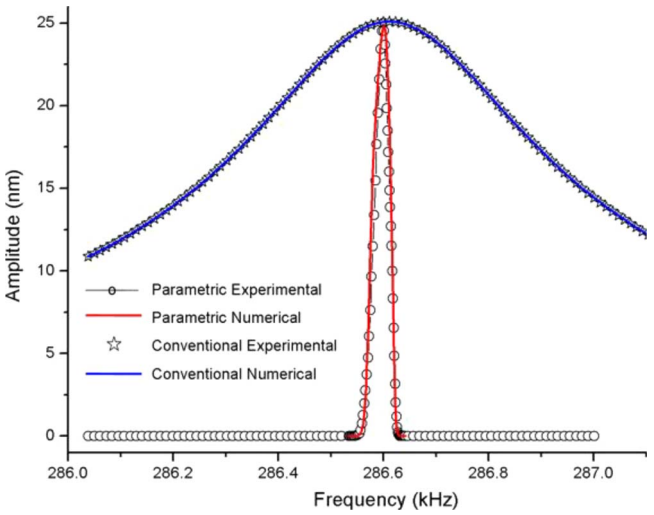

FIG. 2. (Color online) Experimental plot (from Ref. 7) of the frequency response for a conventional and a parametrically excited microcantilever. The data are well fit by the simulation results. For a parametrically excited microcantilever the horizontal axis is half of its excitation frequency whereas for a conventionally excited microcantilever, the horizontal axis represents the excitation frequency. The nonlinear hydrodynamic damping coefficient (α) was estimated by matching the amplitude and bandwidth of the experimental parametric curve. To fit the data, a value of $\alpha=2.62\times10^{-9}$ kg/m is required.

IV. NUMERICAL RESULTS

Before presenting the simulation results for the three different types of microcantilever excitation, the value of the nonlinear fluidic damping coefficient (α) in Eq. (4) is estimated to be 2.62×10^{-9} kg/m, a value obtained by matching the experimental frequency response in Ref. 7 with the theoretical predictions using a gain (G) of 1.0041^*G_{th}. The resulting fit is shown in Fig. 2. Here, G_{th} is the threshold feedback gain required to cancel damping in the system. In order to achieve a self-sustained oscillation, the feedback gain should be greater than the threshold gain $G_{\text{th}}=2/Q$. The microcantilever parameters such as natural frequency $f_0=286.6$ kHz and Q factor $Q=520$ are taken from Ref. 7. The

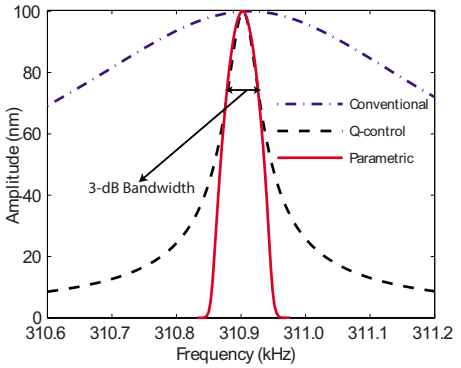

FIG. 3. (Color online) Calculations of the resonance peak for a parametrically excited microcantilever (f_0=310.9 kHz), a Q-controlled microcantilever, and a conventionally excited microcantilever. For the parametrically excited microcantilever, the horizontal axis is half of its excitation frequency whereas for the Q-controlled and the conventionally excited microcantilevers, the horizontal axis represents the excitation frequency. The effective Q factor for the Q-controlled microcantilever is chosen to be Q_{eff}=6000 to match the resonance bandwidth (3 dB width) with that of a parametrically excited microcantilever. The gain for the parametrically excited microcantilever is chosen to be G=1.0139G_{th}.

value for the nonlinear fluidic damping coefficient (α) obtained in this way is used for all further computations. However, for simulation purposes we use the parameters f_0 =310.9 kHz and Q=520 as listed in Table I and G =1.0139*G_{th}. These parameters better represent a standard intermittent contact mode cantilever commonly used in practice.

In order to compare Q-controlled AFM and conventional AFM with parametric AFM on a rational basis, we choose an effective Q factor (Q_{eff}) for the Q-controlled case, so that the resonance bandwidth (defined as the ratio of resonance frequency and 3 dB frequency bandwidth of the peak) is the same as that for parametric resonance. Additionally, the free vibration amplitude (A_0) of the Q-controlled microcantilever oscillation is set equal to that of the parametrically excited microcantilever. Finally, in the case of the conventionally excited microcantilever, the natural Q factor from Table I is used for the simulations while the free amplitude (A_0) of the oscillation is set equal to that of parametric case.

Figure 3 shows a comparison of the frequency response for a parametrically resonant, a Q-controlled, and a conventionally resonant microcantilever. The effective Q-factor required by Q-controlled excitation to match the resonance bandwidth of parametrically excited microcantilever is estimated to be Q_{eff}=6000. The free vibration amplitude of Q-controlled and conventional excitations at resonance is chosen to be same as that of free vibration amplitude of parametric resonance. Unless otherwise stated, all the following simulations are performed with the parameters listed in Table I. In what follows we compare the three excitation mechanisms in terms of (a) peak imaging force, (b) amplitude sensitivity, (c) transient dynamics, and (d) sensitivity to long-range force gradients.

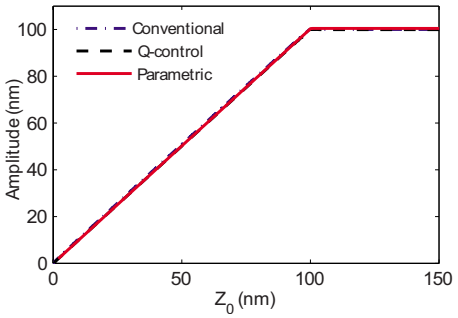

FIG. 4. (Color online) A comparison of the calculated amplitude reduction (approach curve) for a Si tip mounted on a microcantilever as it approaches an HOPG sample. The calculations are performed for parametric, Q-controlled, and conventional microcantilever excitations.

A. Imaging force

As the tip is brought close to the sample, it intermittently interacts with the sample and experiences short- and long-range forces while imaging the topography of the sample. The peak force is defined by the maximum (attractive and repulsive) imaging force per cycle. The value of the peak force reflects important physical properties of the sample such as adhesion, viscoelasticity, and specific chemical interactions.[27,28] Figure 4 provides a comparison between different approach curves (oscillation amplitude A vs Z_0) for three different types of microcantilever excitation. For each approach curve, the imaging force calculated using Eq. (5) depends on the instantaneous tip-sample separation z. The peak forces (attractive and repulsive) plotted in Fig. 5 are the envelope of the imaging force where a positive peak force represents the repulsive force and a negative peak force represents the attractive force.

Figure 5 shows that the peak force in the parametric approach curve is comparable with that of the Q-controlled approach curve. However in the plot for the Q-controlled approach curve, the transition from the attractive to repulsive regime is accompanied by an oscillatory (ringing) transient behavior. In contrast, for parametric resonance the transition from the attractive to the repulsive regime is faster,

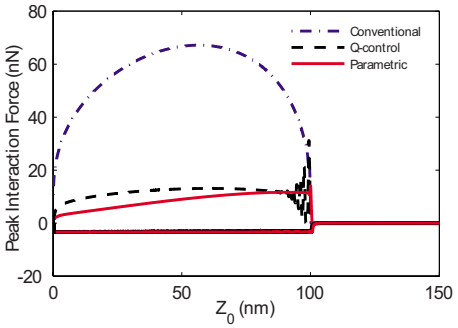

FIG. 5. (Color online) A comparison between the calculated peak interaction forces (attractive: negative and repulsive: positive) between a Si tip and an HOPG sample. The calculations are performed for parametric, Q-controlled, and conventional microcantilever excitations.

smoother, and without ringing transients. The ringing transients in peak force for the Q-controlled case produce an unwanted (and uncontrolled) large interaction force as illustrated in Fig. 5. We also find that the peak repulsive force in the parametric approach curve is an order of magnitude smaller than found for a conventional approach curve. As discussed above, parametric AFM can achieve Q_{eff} as high as 6000, a value about ten times the natural Q factor. It is difficult to implement such a high Q_{eff} in Q-controlled AFM.[29] Nonetheless in order to make a fair comparison with our simulations, we present a comparison of interaction forces and transients for parametric vs Q-controlled AFM using an equal value of $Q_{\text{eff}}=6000$. We have performed several simulations (not shown) that clearly show that these advantages persist so long as Q_{eff} is greater than twice the natural Q factor.

Reduced imaging forces imply reduced indentation of the tip which is critical for scanning soft biological samples. Further simulations show that if the feedback gain G is brought closer to G_{th}, the imaging force becomes purely attractive until the set-point amplitude (A/A_0) is very small. For a conventionally resonant microcantilever, it has been shown that due to the presence of the tip-sample interaction force, there exist two stable oscillation states.[30–33] While approaching the sample, the tip experiences an attractive tip-sample interaction force before encountering an instability. Thereafter the tip experiences the repulsive part of the tip-sample interaction force. On the contrary, for Q-controlled AFM probes with high Q_{eff}, it has been shown that the attractive regime exists over a large range of set-point ratios,[5] so it is possible to approach the sample without transitioning to the repulsive regime. As a consequence, the interaction forces remain small.

For the parametrically resonant probe the situation is similar since as G approaches G_{eff}, the frequency response of the parametrically resonant probe becomes sharper. As a consequence, the probe remains in the attractive regime during the approach to the sample. Thus during approach, the parametrically resonant probe exerts greatly reduced forces similar to the Q-controlled probe. However when the system does transition to the repulsive regime it does so without experiencing significant force transients. With such gentle imaging forces and no ringing, parametric resonance based AFM offers advantages when scanning ultrasoft biological samples.

B. Amplitude sensitivity

Amplitude sensitivity is defined as the slope of the approach curve with respect to approach distance $(\partial A/\partial Z_0)$. Greater amplitude sensitivity implies that larger changes in amplitude (A) will occur due to changes in the tip-sample equilibrium gap (Z_0). This in turn reduces controller effort required to track the sample topography. Thus amplitude sensitivity is directly related to image height resolution.

Upon computing the approach curves for the three cases, we find that the amplitude sensitivity is similar for all three types of excitations as shown in Fig. 6(a), at least for our particular choice of a relatively hard sample (HOPG). When

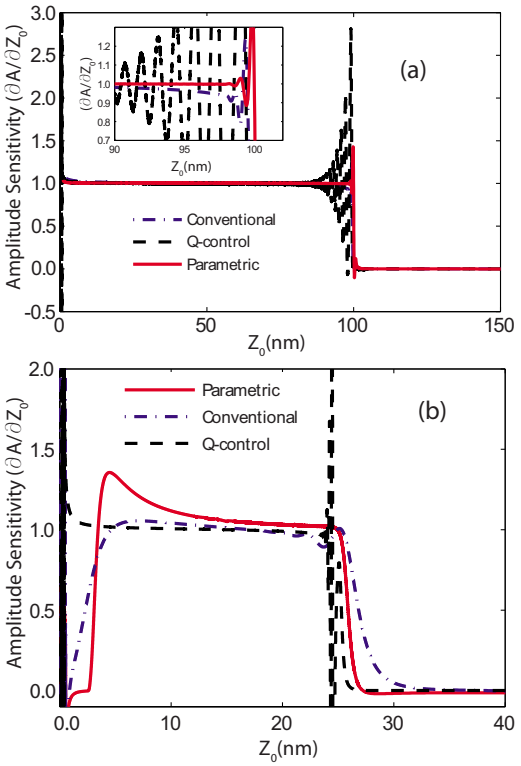

FIG. 6. (Color online) A comparison between the calculated amplitude sensitivity $(\partial A/\partial Z_0)$ for different types of microcantilever excitations at two different feedback gains. The calculations were performed for a Si tip approaching an HOPG sample. In (a), a feedback gain, $G=1.0139G_{\text{th}}$. The inset provides an expanded view of the transient behavior. In (b), a feedback gain, $G=1.0041G_{\text{th}}$.

the tip begins to intermittentantly contact the sample, the amplitude gradient of parametric excitation is slightly better than the conventional excitation, as shown in the inset of Fig. 6(a). However, at lower gain, for example, when $G=1.0041G_{\text{th}}$ and at lower set-point values (~5%–10%), the amplitude sensitivity for the parametrically resonant case improves by 25% as shown in Fig. 6(b).

Thus the parametrically resonating microcantilever shows higher amplitude sensitivity at lower gain values as compared to an equivalent conventional or Q-controlled resonant microcantilever. Furthermore, as discussed above, at lower gain the microcantilever remains in the attractive force regime, enabling a parametric AFM to obtain better height resolution while imaging ultrasoft samples.

C. Transient scanning dynamics

The results of numerically simulating an open-loop line scan are shown in Fig. 7. An open-loop scan is performed in order to understand the dynamics of an oscillating microcantilever by different excitations without any feedback from the controller. The response of the microcantilever to the surface feature shown in Fig. 7(a) is calculated numerically.

To begin, the microcantilever is positioned close to the sample at a fixed Z_0. The microcantilever is allowed to resonate while the tip intermittently interacts with the sample via the tip-sample interaction force [Eq. (5)]. The microcantile-

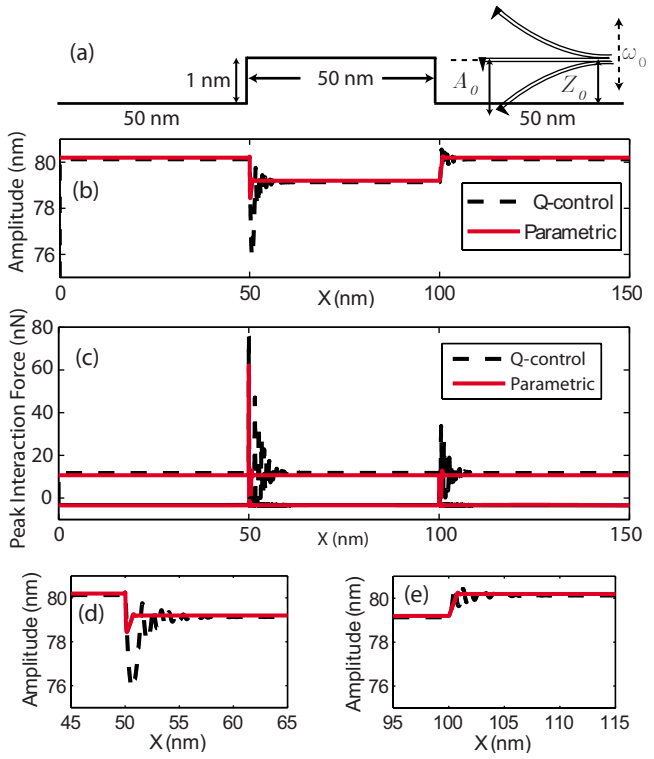

FIG. 7. (Color online) A comparison of a numerically simulated open-loop line scan of a parametric AFM with an equivalent Q-controlled AFM. In (a), a plot of the surface to be scanned. In (b), a plot of the microcantilever oscillation amplitude for a parametric resonance based AFM and a Q-controlled AFM. In (c), a plot of the peak interaction forces (both attractive and repulsive) for both a parametric AFM and a Q-controlled AFM. In (d), a plot showing transients in the amplitude of the microcantilever response of a Q-controlled AFM (broken line) and a parametric AFM (solid line) for the left (step-up) feature. In (e), a similar plot for the right (step-down) feature.

ver is moved across the surface to scan the topography. Any change in the sample's surface is recorded as a change in the amplitude of the resonating microcantilever. In the case of no feedback (an open-loop scan), when the resonating microcantilever tip encounters a surface feature, the controller does not act to correct the amplitude of the microcantilever. The microcantilever naturally oscillates until the transients die out and a steady-state oscillation amplitude is reached. Already in Fig. 5, we provided clear evidence that the tip in conventional AFM exerts an undesirably large force on a sample as compared to other methods. For this reason in this section we only compare parametric AFM with Q-controlled AFM.

A tip, resonating at an equilibrium distance $Z_0=80$ nm from the sample, encounters a step of 1.0 nm height and 50 nm length, as shown in Fig. 7(a). Numerical simulations of the open-loop scan using Q-controlled and parametrically resonating microcantilevers are compared in Fig. 7(b). The details of the transients are plotted in Figs. 7(d) and 7(e) for the left and right steps, respectively. The transient time of open-loop parametric scan is found to be an order of magnitude smaller than that of the open-loop Q-controlled scan. Moreover, as the resonating microcantilever scans the step-down and step-up surface features, the Q-controlled microcantilever exhibits a pronounced ringing transient, in strong contrast to the steplike change in amplitude observed for the parametrically resonating microcantilever. The smaller transient time of a parametrically resonating microcantilever will enable the parametrically resonant AFM to scan faster as compared to a Q-controlled AFM. By comparing the transient response for the two cases plotted in Figs. 7(d) and 7(e), we estimate that the parametrically resonant AFM can scan about a factor of 10 faster than a Q-controlled AFM.

We find that the ringing transients present in a Q-controlled AFM are the main reason behind the undesirably large (and uncontrolled) tip-sample interaction forces evident in Fig. 7(c). The ringing transients that occur when a tip encounters a surface feature in a Q-controlled AFM also require a slower scanning speed as compared to the case of a parametrically resonating microcantilever.

It is useful to discuss why there are ringing transients present in a resonating microcantilever under Q-controlled excitation whereas they are absent in a parametrically resonating microcantilever. From Eq. (4), we find that equation of motion for a parametrically resonating microcantilever is a second-order homogeneous differential equation whose solution grows exponentially until reaching the steady state. On the contrary, the equation of motion for a microcantilever resonating under Q-controlled excitation is an inhomogeneous equation having a particular as well as a homogeneous solution. The amplitude of the particular solution dies out exponentially with time whereas the homogeneous (steady-state) solution provides a fixed amplitude solution for all times. It is important to realize that the two solutions for a Q-controlled microcantilever have slightly different frequencies. These two frequencies generate a beat frequency which results in a ringing transient that persists for a much longer time than the parametrically resonating microcantilever.

D. Sensitivity to the long-range force gradients

In the presence of long-range interaction forces, the stiffness of the microcantilever is modified as

$$k_{\text{eff}} = k_c + dF_{\text{lr}}/dZ_0, \tag{8}$$

where k_c is the microcantilever stiffness, F_{lr} is the long-range interaction force, dF_{lr}/dZ_0 represents the long-range interaction force gradient, and k_{eff} is the effective stiffness of the microcantilever in the presence of the long-range interaction force gradient. Equation (8) provides an operational definition for parametrizing the long-range interaction force gradient. For example, in the presence of an attractive long-range interaction force with $dF_{\text{lr}}/dZ_0 > 0$ the microcantilever will effectively stiffen, increasing the microcantilever resonance frequency. The shift in resonance frequency is a measure of the strength of the long-range interaction force gradient. A positive shift (increased resonance frequency) signals the presence of positive long-range interaction force gradient whereas a negative shift (decreased resonance frequency) indicates the presence of negative long-range force gradient. The shift in the resonance frequency eventually leads to a change in amplitude and phase of the oscillating microcantilever.

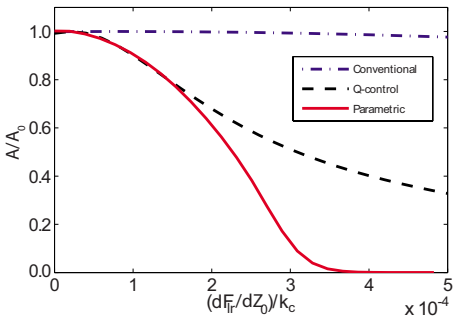

FIG. 8. (Color online) The variation in amplitude of a microcantilever oscillating in the presence of a long-range interaction force gradient. The horizontal axis plots the ratio of the long-range force gradient to the microcantilever stiffness. The vertical axis represents the variation in the normalized amplitude of the probe as the strength of the interaction force gradient increases.

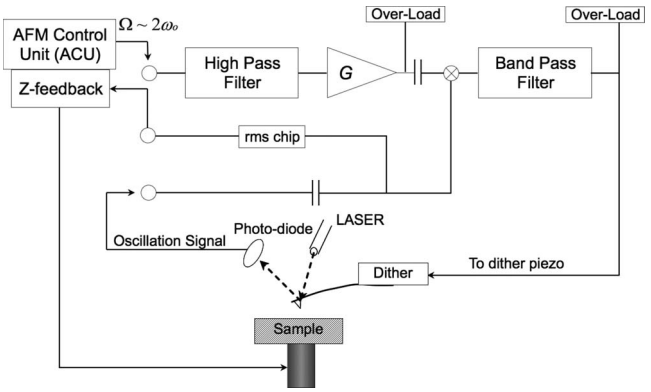

FIG. 9. A block circuit diagram illustrating the essential components required to implement parametric excitation of a microcantilever using electronic feedback.

Figure 8 shows how the normalized amplitude (A/A_0) changes in the presence of a long-range interaction force gradient normalized by the microcantilever stiffness, $\frac{1}{k_c}\frac{dF_{\rm lr}}{dZ_0}$. From Fig. 8, it is apparent that a conventional AFM shows little sensitivity to the long-range force gradient. When the normalized long-range force gradient is less than ~1.5, both Q-control and parametric based AFMs show a similar sensitivity as judged by a change in the normalized amplitude. For normalized force gradients greater than ~3.5, the parametric based AFM looses sensitivity since the normalized amplitude rapidly approaches zero. From the slope of the curves we can infer that when the normalized force gradient lies between 1.5 and 3.5, the change in the normalized amplitude is largest for parametric AFM. Hence we find that measurements of the normalized amplitude using a parametric AFM can provide more sensitivity to long-range interaction force gradients when compared to Q-controlled or conventional AFM.

Both magnetic and electrostatic forces can generate long-range force gradients $dF_{\rm lr}/dZ_0$ close to the surface. Magnetic force microscopy (MFM) and electrostatic force microscopy (EFM) are useful to study magnetic and electric effects at the nanoscale.[34–37] The higher amplitude sensitivity of the parametrically resonant microcantilever to the presence of a long-range interaction force gradient suggests that MFM or EFM performed using a parametrically resonant microcantilever should provide better resolution of magnetic or electric forces at the nanoscale.

V. IMPLEMENTING A PARAMETRIC AFM

An experimental study was independently performed to confirm the numerical findings outlined above. In what follows, we outline the experimental setup and discuss a few relevant experimental results.

A. Experimental considerations

The experimental setup used for implementing parametric resonance in AFM is identical to the one described elsewhere.[7] Briefly parametric excitation is implemented by multiplying, in hardware, the measured microcantilever deflection with a harmonic parametric excitation signal at a drive frequency Ω. The resulting signal is amplified with a gain (called parametric gain, G) and then used to excite the dither piezo.[7] Figure 9 shows a schematic layout of the circuit used to multiply the two signals for a parametric excitation of the microcantilever. By tuning the drive frequency such that $\Omega \sim 2\omega_0$ (ω_0 is the natural frequency of first eigenmode) and increasing the parametric gain G, it is possible to drive the microcantilever into parametric resonance. For imaging purposes, the drive frequency is fixed as the microcantilever approaches the sample. Upon approach, the root-mean-square oscillation amplitude $(A_{\rm rms})$ is reduced. At a certain amplitude reduction (set-point ratio), the scanning controller maintains a constant set-point ratio as the sample is rastered beneath the oscillating microcantilever. It is important to note that unlike conventional AFM where the drive and microcantilever frequency are identical $(\Omega \sim \omega_0)$, in parametric AFM $\Omega \sim 2\omega_0$ so that a lock-in amplifier at the drive frequency cannot be used to detect the cantilever amplitude. Instead, in our implementation we measure $A_{\rm rms}$ and use it as the feedback signal for scanning.

B. Experimental results

The experiments are performed using a stiff microcantilever series: PPP-NCLR from Nanosensors, Switzerland with a nominal stiffness of 48 N/m. Figure 10 shows a measured frequency response of the parametrically resonating microcantilever far from the sample surface demonstrating a $Q_{\rm eff} = 1550$, approximately three times that of the natural Q factor $(Q=520)$. The parametrically resonant microcantilever is used to scan a silicon grating [MikroMash Si grating (TGZ02)] in the amplitude modulated (intermittent contact) mode at an amplitude set-point ratio of 0.6. In implementing these scans it is necessary to correctly choose the proportional (K_P) and integral (K_I) gains which are crucial parameters to minimize the error signal.

In order to identify the set of values for K_P and K_I to minimize the error signal, first K_P was increased keeping K_I constant until imaging instabilities set in. Then K_P is reduced to half the critical value and the value of K_I is systematically increased until the error signal is minimized. Interestingly for

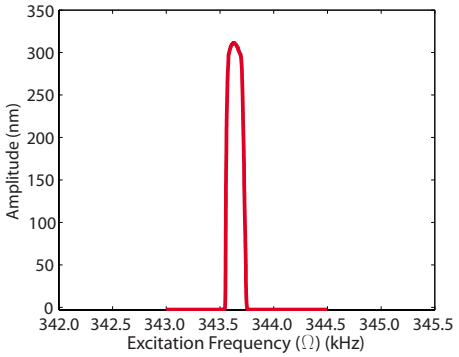

FIG. 10. (Color online) An experimental response curve obtained using the parametric-resonance circuit described in Fig. 9. The nominal stiffness of the microcantilever is 48 N/m. The gain was adjusted to set $Q_{\text{eff}}=1550$, approximately three times the natural Q factor ($Q_{\text{natural}}=520$). Note that parametric resonance occurs when the drive frequency $\Omega \sim 2\omega_0$ (experimental value for $\omega_0=171.83$kHz) as predicted by theory.

this cantilever and image scan size, we find that unlike conventional AFM, where optimal K_P/K_I ratio is about 2, in parametric AFM this ratio is closer to 800.

In Fig. 11 we show a topographic image of a Si grating, along with a line profile for the optimal combination of the K_P and K_I parameters. These experiments clearly demonstrate that the parametrically resonant microcantilever does not exhibit ringing transients as is evident by the smooth edges observed in the topographic profiles despite the scan rate of 1.0 Hz for a image size of 5×5 μm^2 with a $Q_{\text{eff}}=1550$. The absence of the ringing transients despite the higher Q_{eff} confirms the simulation results described in Sec. IV above.

The experiments have also allowed us to better identify some of the challenges in the routine experimental implementation of a parametric AFM. Under ambient conditions, approaching the sample at very high Q_{eff} (Q_{eff} greater than three times the natural Q factor) is a problem because the air damping between the microcantilever and the sample increases slightly upon approach due to squeeze film effects. As a consequence, at some point during the approach, the parametric gain falls below the threshold value required to sustain parametric resonance. This can be avoided by using lower Q_{eff}. Second, we have found that achieving small free vibration amplitudes (less than 50–100 nm) is difficult due to the high sensitivity of the microcantilever's oscillation amplitude to parametric gain.

VI. SUMMARY AND CONCLUSIONS

In summary, we find that parametric resonance is a promising way to excite an AFM probe in a narrow frequency bandwidth. Parametric AFM has a number of distinct advantages over Q-controlled AFM such as sharp resonance bandwidth and low tip-sample interaction forces without incurring the disadvantages of Q-controlled AFM such as unwanted ringing effects and slow scanning speeds. Based on simulations, parametric AFM exhibits a lower tip-sample interaction force, reduced cantilever transients, and an improved amplitude sensitivity in the presence of long-range interaction forces as compared to Q-controlled and conventional AFMs. Experimental results using a parametric AFM confirm the absence of ringing transients at higher Q_{eff}. Taken together these results suggest that parametrically resonant cantilevers offer distinct advantages over other dynamic AFM techniques, especially with regard to reduced imaging forces and reduced transients.

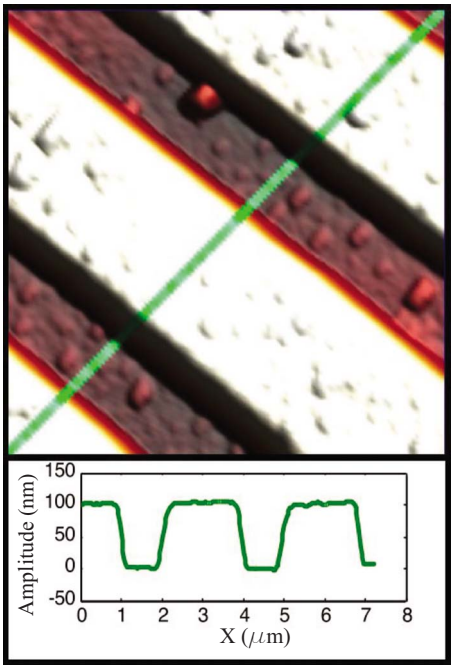

FIG. 11. (Color online) An AFM image of a MikroMasch silicon grating (TGZ02) imaged by a parametric AFM with an amplitude set-point ratio of $0.6A_{\text{rms}}$. Scan rate is 1.0 Hz. The figure demonstrates that at typical scan rates, there are minimal ringing transients at the edges in spite of a high $Q_{\text{eff}}=1550$. The image size is 5×5 μm^2. A topographic profile along the diagonal line is shown in the inset.

ACKNOWLEDGMENTS

The authors thank the National Science Foundation (NSF) for their financial support in part through Grant No. 0700289.

[1] J. Kokavecz, Z. L. Horvathoth, and Á. Mechler, Appl. Phys. Lett. **85**, 3232 (2004).
[2] D. Ebeling, H. Hölscher, H. Fuchs, B. Anczykowski, and U. D. Schwarz, Nanotechnology **17**, S221 (2006).
[3] J. Tamayo, J. Appl. Phys. **97**, 044903 (2005).
[4] T. R. Rodriguez and R. Garcia, Appl. Phys. Lett. **82**, 4821 (2003).
[5] H. Hölscher, D. Ebeling, and U. D. Schwarz, J. Appl. Phys. **99**,

084311 (2006).
[6] J. Mertz, O. Marti, and J. Mlynek, Appl. Phys. Lett. **62**, 2344 (1993).
[7] M. Moreno-Moreno, A. Raman, J. Gomez-Herrero, and R. Reifenberger, Appl. Phys. Lett. **88**, 193108 (2006).
[8] T. Ouisse, M. Stark, F. Rodrigues-Martins, B. Bercu, S. Huant, and J. Chevrier, Phys. Rev. B **71**, 205404 (2005).
[9] M. V. Requa and K. L. Turner, Appl. Phys. Lett. **88**, 263508 (2006).
[10] S. Patil and C. V. Dharmadhikari, Appl. Surf. Sci. **217**, 7 (2003).
[11] M. Faraday, Philos. Trans. R. Soc. London **121**, 299 (1831).
[12] N. D. Naumov and Yu. G. Pavlenko, Tech. Phys. **42**, 22 (1997).
[13] S. M. Curry, Am. J. Phys. **44**, 924 (1976).
[14] K. L. Turner, S. A. Miller, P. G. Hartwell, N. C. Macdonald, S. H. Strogatz, and S. G. Adams, Nature (London) **396**, 149 (1998).
[15] M. F. Yu, G. J. Wagner, R. S. Ruoff, and M. J. Dyer, Phys. Rev. B **66**, 073406 (2002).
[16] A. H. Nayfeh and D. T. Mook, *Nonlinear Oscillations* (Wiley, New York, 1979).
[17] D. Rugar and P. Grutter, Phys. Rev. Lett. **67**, 699 (1991).
[18] W. M. Dougherty, K. J. Bruland, J. L. Garbini, and J. A. Sidles, Meas. Sci. Technol. **7**, 1733 (1996).
[19] A. Dâna, F. Ho, and Y. Yamamoto, Appl. Phys. Lett. **72**, 1152 (1998).
[20] J. Melcher, S. Hu, and A. Raman, Appl. Phys. Lett. **91**, 053101 (2007).
[21] E. Mathieu, J. Math. Pures Appl. **18**, 137 (1868).
[22] R. Rand, *Lecture Notes on Nonlinear Vibration* (Internet-First University Press, Ithaca, 2003) (http://audiophile.tam.cornell.edu/randdocs/nlvibe52.pdf).
[23] B. V. Derjaguin, V. M. Müller, and Y. P. Toporov, J. Colloid Interface Sci. **53**, 314 (1975).
[24] U. M. Ascher and L. R. Petzold, *Computer Methods for Ordinary Differential Equations and Differential-Algebraic Equations* (SIAM, Philadelphia, 1999).
[25] P. N. Brown, A. C. Hindmarsh, and L. R. Petzold, SIAM J. Sci. Comput. (USA) **15**, 1467 (1994).
[26] P. N. Brown, A. C. Hindmarsh, and L. R. Petzold, SIAM J. Sci. Comput. (USA) **19**, 1495 (1998).
[27] F. J. Giessibl, Phys. Rev. B **56**, 16010 (1997).
[28] S. Hu and A. Raman, Appl. Phys. Lett. **91**, 123106 (2007).
[29] P. D. Ashby, Appl. Phys. Lett. **91**, 254102 (2007).
[30] R. Garcia and A. San Paulo, Phys. Rev. B **60**, 4961 (1999).
[31] A. San Paulo and R. Garcia, Phys. Rev. B **66**, 041406(R) (2002).
[32] S. I. Lee, S. W. Howell, A. Raman, and R. Reifenberger, Phys. Rev. B **66**, 115409 (2002).
[33] L. Zitzler, S. Herminghaus, and F. Mugele, Phys. Rev. B **66**, 155436 (2002).
[34] Y. Martin, C. C. Williams, and H. K. Wickramasinghe, J. Appl. Phys. **61**, 4723 (1987).
[35] D. Rugar, H. J. Mamin, P. Guethner, S. E. Lambert, J. E. Stern, I. McFadyen, and T. Yogi, J. Appl. Phys. **68**, 1169 (1990).
[36] C. Schönenberger and S. F. Alvarado, Phys. Rev. Lett. **65**, 3162 (1990).
[37] D. W. Abraham, C. Williams, J. Slinkman, and H. K. Wickramasinghe, J. Vac. Sci. Technol. B **9**, 703 (1991).